BIOCHEMISTRY
including biophysical chemistry & molecular biology

Article

pubs.acs.org/biochemistry

A Flexible Glutamine Regulates the Catalytic Activity of Toluene *o*-Xylene Monooxygenase

Alexandria Deliz Liang, Alexandra T. Wrobel, and Stephen J. Lippard*

Department of Chemistry, Massachusetts Institute of Technology, Cambridge, Massachusetts 02139, United States

Supporting Information

ABSTRACT: Toluene/*o*-xylene monooxygenase (ToMO) is a bacterial multicomponent monooxygenase capable of oxidizing aromatic substrates. The carboxylate-rich diiron active site is located in the hydroxylase component of ToMO (ToMOH), buried 12 Å from the surface of the protein. A small, hydrophilic pore is the shortest pathway between the diiron active site and the protein exterior. In this study of ToMOH from *Pseudomonas* sp. OX1, the functions of two residues lining this pore, N202 and Q228, were investigated using site-directed mutagenesis. Steady-state characterization of WT and the three mutant enzymes demonstrates that residues N202 and Q228 are critical for turnover. Kinetic isotope effects and pH profiles reveal that these residues govern the kinetics of water egress and prevent quenching of activated oxygen intermediates formed at the diiron active site. We propose that this activity arises from movement of these residues, opening and closing the pore during catalysis, as seen in previous X-ray crystallographic studies. In addition, N202 and Q228 are important for the interactions of the reductase and regulatory components to ToMOH, suggesting that they bind competitively to the hydroxylase. The role of the pore in the hydroxylase components of other bacterial multicomponent monooxygenases within the superfamily is discussed in light of these conclusions.

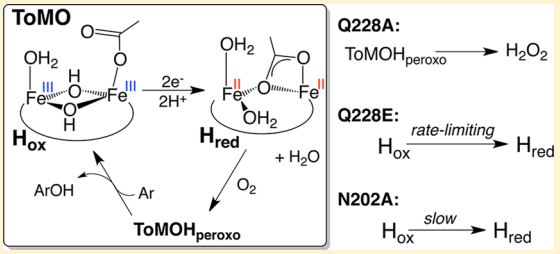

Bacterial multicomponent monooxygenases (BMMs) comprise a family of enzymes capable of hydroxylating and epoxidizing hydrocarbon substrates at carboxylate-rich diiron active sites. Bacteria containing BMMs help to regulate the global carbon cycle[1] and are used for bioremediation of environments contaminated with hydrocarbons and halogenated pollutants.[2,3] All BMMs require a hydrocarbon substrate, molecular oxygen, protons, and electrons acquired through NAD(P)H.[4] Each BMM requires either three or four components that must reversibly bind one another throughout catalysis. Dynamic interactions among these protein components orchestrate substrate delivery to their diiron centers and subsequent catalytic turnover.[5−8] Toluene/*o*-xylene monooxygenase (ToMO) is a four-component, arene-oxidizing BMM composed of an NADH-oxidoreductase (ToMOF), a Rieske-type ferredoxin (ToMOC), a cofactorless regulatory protein (ToMOD), and the catalytic hydroxylase protein (ToMOH). Three component BMMs, like soluble methane monooxygenase (sMMO), lack the Rieske-type ferredoxin.

The diiron active sites in the 200−250 kDa hydroxylase components of BMMs are buried ∼12 Å from the protein surface within a four-helix bundle.[9] The extensive protein architectures of these hydroxylase components protect intermediates formed during dioxygen activation from undesired side reactions, but they also provide a barrier to direct substrate access. This potential problem is addressed by channels and interconnected cavities that traverse the hydroxylase. These cavities and channels provide access of dioxygen[10,11] and hydrocarbons[12,13] to the diiron active sites, as revealed by X-ray crystallographic studies of four BMMs: ToMO, toluene-4-monooxygenase (T4MO), soluble methane monooxygenase (sMMO), and phenol hydroxylase (PH). A conserved pore comprising the shortest distance from the diiron site to the solvent-exposed surface has been discovered within all crystallographically characterized BMMs but has not yet been functionally investigated. This pore is lined by three hydrophilic residues: a threonine, an asparagine, and either a glutamate or glutamine (Figure 1).[14−16]

X-ray crystallographic studies revealed that the pore is hydrophilic[12] and flexible[14,15] and can accommodate an ordered water molecule, designated HOH5,[13,14] when the regulatory protein is bound to the hydroxylase. These structural results strongly suggest a role for the conformationally flexible, surface-exposed pore in the catalytic function of these enzymes. Proposals for this function include mediating proton transfer (PT)[9,14] or proton-coupled electron transfer (PCET)[15] and providing a pathway for water or hydroxylated products to exit the active site.[12]

In the present study, we evaluate reactivity changes following site-directed mutagenesis of residues within the pore of ToMOH from *Pseudomonas* sp. OX1, the hydroxylase of a canonical four-component BMM that displays moderate regiospecificity during aromatic hydroxylation.[17] Steady-state and pre-steady-state studies demonstrate that residues N202 and Q228 of ToMOH are critical for efficient turnover, water

Received: March 29, 2014
Revised: May 10, 2014
Published: May 29, 2014

   dx.doi.org/10.1021/bi500387y | *Biochemistry* 2014, 53, 3585−3592

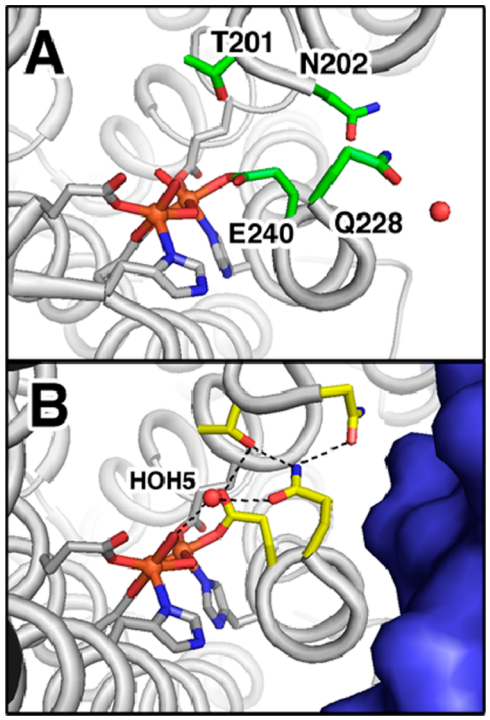

Figure 1. Conformationally flexible pore of T4MO. Binding of the regulatory protein to the hydroxylase of T4MO elicits structural changes within the pore. The unbound, oxidized hydroxylase (PDB: 3DHG) and the complex between the regulatory protein and the oxidized hydroxylase (PDB: 3DHH) are shown in panels A and B, respectively. The regulatory protein in panel B is depicted as a blue surface. The hydroxylase is colored in gray, cut away to highlight the pore and diiron active site. The active site, drawn as sticks, is colored by atom type: carbon (gray), oxygen (red), nitrogen (blue), and iron (orange). Carbon atoms of the pore appear in green and yellow to emphasize the conformational changes. Hydrogen bonds (varying between 2.7 and 2.9 Å) between the pore residues, active site ligands, and water molecule HOH5 are indicated by dashed black lines. Water molecules near or within the pore are shown as red spheres.

egress from the active site, protection of intermediates formed during oxygen activation, and binding of the electron transfer protein, ToMOC, to the hydroxylase. We propose that these activities are achieved through movement of residues N202 and Q228 during catalysis.

MATERIALS AND METHODS

Materials and General Methods. Wild-type (WT) vectors were kindly provided by Prof. Alberto Di Donato, Naples, Italy. Chromatography was conducted in a cold room maintained at 4 °C. Catechol 2,3-dioxygenase (C23O) was used in coupled activity assays as previously described.[18] Protein images and cartoon representations of mutants were rendered using PyMOL X11/Hybrid.[19] Tris, Bis-Tris, and phosphate salts were purchased from CalBioChem, Santa Cruz Biochemical, and BDH, respectively. NADH was obtained from Roche. Phenol and sodium dithionite were purchased from Sigma-Aldrich.

Expression and Purification of ToMO Components. Expression and purification methods for ToMOH, ToMOD, and ToMOC were modified from previously reported procedures, as detailed in the Supporting Information.[16,18] ToMOF was expressed and purified as previously described.[20] Details for the preparation of mutants N202A, Q228A, and Q228E are included in the Supporting Information.

NADH Consumption Assays. A 350 μL solution comprising 0.15 μM WT or mutant hydroxylase, 6 μM ToMOD, 6 μM ToMOC, 60 nM ToMOF, and 0−1500 μM phenol was prepared in 0.1 M Tris, pH 7.3. The protein mixture was allowed to stand at room temperature for 1 h. The reaction was initiated by addition of NADH (ε_{340} = 6220 M^{-1} cm^{-1}) to a final concentration of 200 μM. The absorbance change at 340 nm, corresponding to NADH consumption, was monitored at 25 °C using a Hewlett-Packard diode array spectrophotometer scanning every 3 s. Initial velocities were obtained by fitting five time points to a linear function. A minimum of three replicates was performed for each condition to obtain standard deviations.

Catechol Formation Assays. The rate of catechol formation was determined by a coupled assay.[18] Reactions were prepared as described for the NADH consumption assay except that excess C23O was added to convert catechol to 2-hydroxymuconic semialdehyde (ε_{410} = 12 620 M^{-1} cm^{-1}). The initial rate of 2-hydroxymuconic semialdehyde was recorded as a function of absorbance at 410 nm over time. For experiments carried out in deuterated buffer, we use D_2O purchased from Icon Isotopes, 99.8% isotope enriched. Before performing pH readings of D_2O-containing buffers, the pH meter probe was soaked in this solvent. The pD value of each D_2O buffer was calculated by adding 0.4 to the pH meter readings. To vary the viscosity of the reaction buffer, 0−1.25 *m* sucrose was added to the buffer. To examine the effect of ToMOC concentration, the rate of turnover with respect to ToMOC concentration was determined using 1−12 μM ToMOC in the steady-state assays.

Steady-State Data Analysis. Initial velocities were plotted against phenol concentration, and the resulting curves were fitted in OriginLabs 9.0 to either the Michaelis−Menten equation or a modified Michaelis−Menten equation accounting for substrate inhibition.[21] Double reciprocal plots were used to calculate the enzymatic efficiencies, k_{cat}/K_m, for each hydroxylase. Graphical representations of the data analysis are shown in Figure S2. The kinetic solvent isotope effects (KSIEs) were derived by dividing k_{cat} or k_{cat}/K_m obtained in H_2O by those obtained in D_2O. Coupling efficiencies were calculated and defined as the rate of product formation divided by the rate of NADH consumption. In assays with varying concentrations of ToMOC, the initial rates were plotted as a function of ToMOC concentration. These plots were fit to the Michaelis−Menten equation with ToMOC as the substrate to determine the k_{cat} and k_{cat}/K_m with respect to ToMOC.

Discontinuous Catechol Formation Assays. To determine the pH profile of WT ToMOH and mutant Q228A, a discontinuous catechol formation assay was used, monitoring the initial rate of catechol formation as a function of pH (Figure S2). A 300 μL solution of 0.15 μM ToMOH WT or Q228A, 6 μM ToMOD, 6 μM ToMOC, 60 nM ToMOF, and 200−500 μM phenol was prepared in 0.1 M Bis-Tris propane, pH 5.75−7.50. The protein mixture was allowed to stand at room temperature for 1 h. The reaction was initiated by addition of NADH to a final concentration of 200 μM. In 10−30 s increments, aliquots of 50 μL were removed from the reaction and quenched in 50 μL of 0.4 M trichloroacetic acid, with the acidified mixture being vigorously pipetted. Five time points were obtained for each condition. The quenched mixture was centrifuged (2000*g*), and the supernatant was diluted 4-fold into buffer containing 500 mM Tris and 50 mM MOPS at pH

dx.doi.org/10.1021/bi500387y | *Biochemistry* 2014, 53, 3585−3592

Table 1. Kinetic Parameters of Hydroxylase Variants

	WT	N202A	Q228A	Q228E
$k_{cat,\ phenol}$ (s^{-1})	4.1(1)	0.59(3)	0.42(6)	0.058(3)
$k_{cat}/K_{m,\ phenol}$ ($mM^{-1}\ s^{-1}$)	220(8)	62.7(9)	16(1)	0.72(5)
KSIE($k_{cat,\ phenol}$)	2.0(1)	1.9(2)	12(1)	0.19(1)
KSIE($k_{cat}/K_{m,\ phenol}$)	0.48(9)	0.24(9)	7(2)	0.018(2)
coupling efficiency	0.98(4)	0.57(3)	0.53(1)	0.39(7)
$k_{cat,\ ToMOC}$ (s^{-1})	9.8(4)	7.8(3)	4.7(7)	0.8(2)
$k_{cat}/K_{m,\ ToMOC}$ ($\mu M^{-1}\ s^{-1}$)	1.04(1)	0.412(8)	0.203(4)	0.019(1)
electron transfer k_{obs} (s^{-1})	44(2)	21.4(4)	40(10)	6(1)

7.3. C23O (5 U) was added to each of the diluted solutions. The absorbance at 374 nm was graphed as a function of the quenching time (2-hydroxymuconic semialdehyde, ε_{374} = 33 000 $M^{-1}\ cm^{-1}$). Linear fits were obtained for each time-course. The k_{cat} and relative coupling efficiency values were plotted as a function of pH and fit to eqs 1 and 2 for WT ToMOH and mutant Q228A, respectively.[22]

$$v\ (s^{-1}) = \frac{y_{max}}{\left(1 + \frac{10^{-pH}}{10^{-pK_{a1}}} + \frac{10^{-pK_{a2}}}{10^{-pH}}\right)} \quad (1)$$

$$v\ (s^{-1}) = \frac{y_{max}}{\left(1 + \frac{10^{-pH}}{10^{-pK_{a1}}}\right)} \quad (2)$$

The coupling efficiency as a function of pH was determined by dividing the rate of catechol formation obtained from the discontinuous assay by the rate of NADH consumption. Because one method is continuous and the other is discontinuous, the coupling efficiencies were normalized to the value at pH 7.25, the pH closest to that used in other steady-state experiments reported here.

Electron Transfer (ET) from ToMOC$_{red}$ to Hydroxylase Variants. ET from reduced ToMOC (ToMOC$_{red}$) to the oxidized hydroxylase variants was monitored by stopped-flow UV−visible spectroscopy configured with a single-wavelength photomultiplier and a tungsten lamp. All stopped-flow data reported were obtained by using a Hi-Tech Scientific (Salisbury, UK) SF-61 DX2 stopped-flow spectrophotometer. Absorbance changes at 458 and 565 nm were monitored, corresponding to the greatest change of extinction coefficient upon oxidation or reduction, ∼4000 and 2000 $M^{-1}\ cm^{-1}$, respectively. Anaerobic preparation of protein samples and the stopped-flow instrument are detailed in the Supporting Information.

The reaction temperatures were maintained at 13 °C with a circulating water bath. The final protein concentrations were 10 μM ToMOC$_{red}$ and 100 μM of the oxidized hydroxylase variant. All data presented are the result of an average of three or more individual mixes of the ET complex. In OriginLabs 9.0 and Kinetic Studio, the data were fit to a single exponential function, eq 3, where C is the initial absorbance, A is the overall absorbance change, k is the rate constant, and t is time.

$$Abs_{458nm}(t) = Ae^{-kt} + C \quad (3)$$

RESULTS

General Steady-State Kinetics. Table 1 and Figures S2−S4 summarize the results of phenol conversion to catechol for WT ToMOH as well as mutants N202A, Q228A, and Q228E. Compared to that of WT ToMOH, the k_{cat} and k_{cat}/K_m values were significantly diminished for the mutant proteins. N202A and Q228A retained 15 and 10% of the WT ToMOH k_{cat}, respectively. ToMOH mutant Q228E exhibited the lowest k_{cat}, only 1.5% that of the WT protein. The most deleterious mutations with respect to catalytic efficiency were Q228A and Q228E, which dropped to 7 and 0.3% of the WT values, respectively. The N202A mutant retained 28% of the catalytic efficiency of WT ToMOH.

WT ToMOH and mutant N202A each displayed similar KSIE(k_{cat}) values. Mutant Q228A exhibited a much larger KSIE(k_{cat}), suggesting that a proton-transfer or viscosity-dependent event is rate-limiting. Conversely, mutant Q228E had a strong inverse KSIE(k_{cat}). Inverse KSIE(k_{cat}/K_m) values were observed with varying magnitudes for all hydroxylase mutants except that of Q228A.

The rate of hydroxylation versus the rate of NADH consumption (coupling efficiency) for WT ToMOH was near unity. Coupling efficiencies for mutants N202A and Q228A decreased to 50%. ToMOH mutant Q228E exhibited the lowest coupling efficiency, 39%. During the course of these experiments, it was noted that decreasing the reaction temperature led to higher coupling efficiencies for mutant Q228A. The source of this increased coupling efficiency may arise from a decreased rate of water flux to the active site as discussed below, but this effect was not further explored (data not shown).

Steady-State Viscosity Dependence. A plot of k_{cat} as a function of viscosity is shown in Figures 2 and S5 for each hydroxylase mutant. Within the viscosity range assayed, the activity did not change significantly for WT ToMOH or mutants N202A and Q228E. With increasing viscosity, the k_{cat} for mutant Q228A decreased dramatically, such that the activity was lowered by more than a factor of 2 at a sucrose molality of 1 or η/η_{rel} of ∼3.3.

Effect of ToMOC on Steady-State Parameters. For WT ToMOH and each mutant enzyme system described here, the steady-state parameters as a function of ToMOC concentration are shown in Table 1 and Figure S6. The enzymatic efficiencies with respect to ToMOC were significantly reduced for all mutants compared to that of WT ToMOH. The errors associated with the steady-state parameters for mutant Q228E are higher than those for other mutants. Even at 25 μM ToMOC, the curve did not begin to saturate for ToMOC variation experiments with mutant Q228E. It was not possible to use higher concentrations of ToMOC owing to interference of the absorbance features of ToMOC with that of NADH and the catechol degradation product, 2-hydroxymuconic semialdehyde.

Steady-State pH Profiles. Figures 3 and S7 depict the steady-state pH dependence of both WT ToMOH and mutant

dx.doi.org/10.1021/bi500387y | Biochemistry 2014, 53, 3585−3592

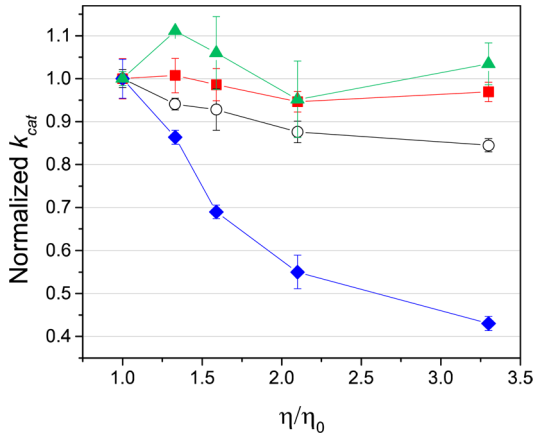

Figure 2. Viscosity dependence of k_{cat} with respect to phenol, normalized to the viscosity of the buffered solution for WT ToMOH (black, open circles), N202A (red squares), Q228A (blue diamonds), and Q228E (green triangles). Turnover was monitored by the catechol formation assay. The reactions were buffered in 0.1 M Tris buffer, pH 7.3, at 25 °C with sucrose as the viscogen. The solution viscosity at each sucrose molality assayed was determined on the basis of previous reports at 25 °C.[23] Non-normalized data are shown in Figure S5.

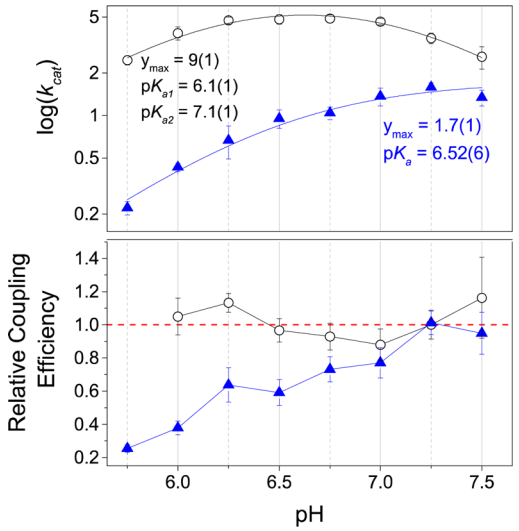

Figure 3. Steady-state pH profiles of WT ToMOH (black, open circles) and mutant Q228A (blue triangles). The reactions were buffered in 0.1 M Bis-Tris propane, pH 5.75−7.5, at 25 °C. Reactions were assayed by both the discontinuous catechol formation and NADH consumption methods. (Top) Maximum rate of product formation as a function of pH with fits according to eqs 1 and 2. (Bottom) Coupling efficiency relative to coupling at pH 7.25 of WT ToMOH and mutant Q228A. The dotted red line indicates full coupling efficiency relative to the coupling efficiency at pH 7.25. The non-normalized data are shown in Figure S7.

Q228A. Concentrations of phenol were varied in these experiments to determine both k_{cat} and k_{cat}/K_m for catechol formation. Although an approximate k_{cat} could be obtained, determination of k_{cat}/K_m was not successful owing to high errors at low concentrations of phenol. The pK_a values derived from fits according to the Materials and Methods are indicated in the top panel of Figure 3. WT ToMOH exhibits two pK_a values within the assayed region, resulting in a bell-shaped curve. The pK_{a1} of mutant Q228A shifts to a higher value, and the pK_{a2} is either not apparent during catalysis or has moved outside of the accessible pH window.

The coupling efficiency as a function of pH is shown in the lower panel of Figure 3. Within error, the WT ToMOH coupling efficiency is near unity for all pH values observed. The coupling efficiency for mutant Q228A decreases significantly with decreasing pH.

Pre-Steady-State ET Kinetics of Hydroxylase Variants. The ET kinetics of each mutant were measured by stopped-flow UV−visible spectroscopy (Table 1, lower panel and Figures S8 and S9). All of the data obtained fit well to a single exponential function based on the quality of the residuals, the adjusted R-squared value, and the error in the fitted parameters. The residuals for the single exponential fit did not oscillate, indicating that a single kinetic event sufficiently described the data. The rate constants for the observed kinetics were similar for WT ToMOH and mutant Q228A. The rate constant decreased by a factor of 2 upon mutation of N202 to alanine and by approximately 8-fold for mutant Q228E.

DISCUSSION

The function of pore residues has generated much speculation since an early Xe-pressurized crystal structure analysis of the hydroxylase of sMMO (sMMOH).[12] Similar to that of other BMM hydroxylases, the pore of ToMOH is surrounded by a dynamic hydrogen-bonding network that includes active site water molecules, the shifting carboxylate E231 ligated to the diiron active site, and amino acids T201, N202, and Q228 (Figure 1).[13,24] The role of the conserved threonine residue, T201, has been a subject of extensive investigation.[20,25−28] The roles of residues N202 and Q228, however, have received far less attention in the literature. To investigate the roles of residues N202 and Q228, we used site-directed mutagenesis and comparative kinetic analysis between WT ToMOH and three hydroxylase mutants, N202A, Q228A, and Q228E. Alanine mutations were selected to definitively disrupt the hydrogen-bonding network surrounding the pore. Mutant Q228E was prepared to mimic the pore of sMMOH, which contains a glutamate instead of a glutamine at this key position (Figure S1).

Experimental Design. ToMO is capable of hydroxylating a wide variety of arene substrates, including toluene, *o*-xylene, benzene, halogenated aromatics, and phenol.[29] Hydroxylation of phenol by ToMO yields only one product, catechol,[29] whereas hydroxylation of toluene leads to a distribution of products, *o*-, *m*-, and *p*-cresol.[17] Owing to its solubility and ease of characterization, phenol was used as the substrate in the steady-state reactions described here.

With respect to turnover, there are two competing processes, as illustrated in Scheme 1, namely, substrate hydroxylation by $ToMOH_{peroxo}$[29] and loss of H_2O_2 from $ToMOH_{peroxo}$. In this work, we examined the efficiency of hydroxylation versus uncoupled activity (H_2O_2 formation).

Two important factors contributing to coupling efficiencies are the concentrations of a hydrocarbon substrate and the function of the regulatory protein, ToMOD. At subsaturating concentrations of either a hydrocarbon substrate or the regulatory protein, the coupling efficiency decreases for many BMMs.[5,30,31] These two factors were kept in mind when designing and interpreting the experiments.

N202 and Q228 Are Critical for Hydroxylation and Coupling Efficiency. For all three mutants, both the rate of product formation and the coupling efficiency were deleteriously affected. To determine whether a lower affinity for

dx.doi.org/10.1021/bi500387y | *Biochemistry* 2014, 53, 3585−3592

Scheme 1. Hydroxylation (Blue) And Loss of Hydrogen Peroxide (Green)

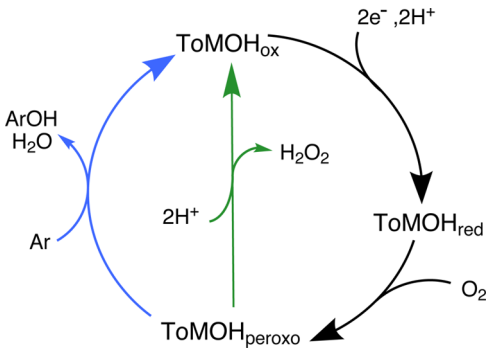

ToMOD was the source of low coupling efficiency, we investigated directly the binding of ToMOH with fluorescein-labeled ToMOD (ToMOD-Fl, see Supporting Information protocols and Figure S10 for details). Mutants N202A and Q228A each retained similar affinities for ToMOD-Fl as that of WT ToMOH. In contrast, mutant Q228E exhibits a diminished binding strength for ToMOD-Fl. Because WT ToMOH and mutants N202A and Q228A maintain a similar ToMOD-Fl binding affinity, the loss of coupling efficiency in these mutants cannot be attributed to a decreased binding affinity for the regulatory protein. Therefore, residues N202 and Q228 must participate in aromatic hydroxylation by ToMOH$_{peroxo}$ (Scheme 1, blue) or downregulate hydrogen peroxide release (Scheme 1, green). This attenuation of activity clearly demonstrates that both N202 and Q228 are critical for efficient hydroxylation.

Residue Q228 Mediates Proton Flux to the Active Site. Identification of HOH5 within the pore of the cognate hydroxylase of T4MO by X-ray crystallography[14] suggests that solvent-mediated PT may occur through the pore. If solvent-derived protons are responsible for a rate-limiting PT step, the observed kinetics will be diffusion-limited and highly sensitive to protium/deuterium solvent exchange.[32] To examine the sensitivity of mutants N202A, Q228A, and Q228E to these variables, product formation assays were conducted monitoring KSIEs, viscosity dependence, and pH dependence.

Of the mutants examined here, only Q228A exhibited a steady-state viscosity dependence and isotope effects greater than two (Figure 2). Because the viscosity of deuterated water is greater than that of protiated water, viscosity-dependent kinetics can also result in KSIE values greater than 1. At the viscosity of deuterated water (n_{rel}, 1.23 mPa S[23]), the k_{cat} of WT and the three mutants varied from 88 to 108% of the k_{cat} in non-sucrose-containing buffer. Thus, viscosity can contribute only a maximum KSIE effect of 1.14 for all mutants. The observed KSIE(k_{cat}) and KSIE(k_{cat}/K_m) values for mutant Q228A are much larger, however, 12 and 7, respectively. Thus, the rate-limiting reaction of mutant Q228A is sensitive to both viscosity and hydrogen−deuterium exchange.

To further examine the proton dependence of mutant Q228A, pH profile studies for catechol formation were carried out with either WT ToMOH or mutant Q228A. The pH profile of WT ToMOH displays a bell-shape (Figure 3), indicating that two prototropic groups are critical for catalysis. The pK_{a1} and pK_{a2} values of WT enzyme are 6.1 and 7.1, respectively. The functional groups responsible for these pK_a values are unknown but may include a histidine side chain (pK_a ~ 6.1), an iron-aqua species (pK_a <15, but widely variable),[33] or a diiron-peroxo species (pK_a ~ 7.2).[34] The coupling efficiency of WT ToMOH did not vary significantly over the pH range investigated (Figure 3). Conversely, the pH profile of mutant Q228A is alkaline-shifted (pK_a ~ 6.52) from that of WT (pK_a ~ 6.1) and did not exhibit a bell-shape within the accessible pH range. At the lower end of the pH range, mutant Q228A displayed significant uncoupling in parallel with the diminished k_{cat} values for conversion of phenol to catechol (Figure 3).

Because the kinetic properties of the Q228A mutant respond to protium−deuterium substitution, the pH of the buffer, and solvent viscosity, we conclude that unregulated solvent-derived proton transfer occurs when the carboxamide side chain is removed in mutant Q228A. We propose that movement of the Q228 side chain attenuates proton flux from solvent, preventing the quenching of oxygenated intermediates in the ToMOH reaction cycle. Figure 4 (bottom panel) illustrates in cartoon

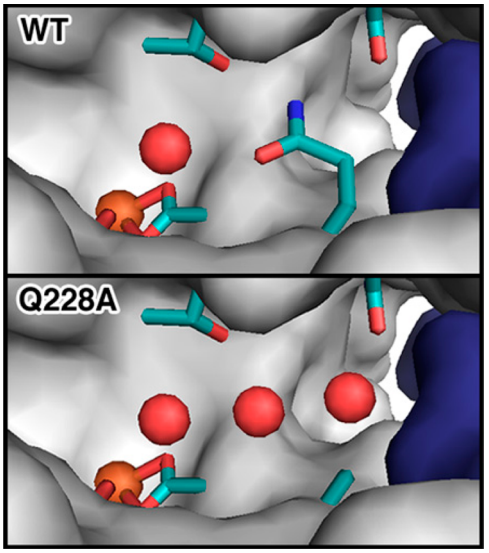

Figure 4. Model for explaining the behavior of mutant Q228A during steady-state turnover. The X-ray crystal structure of the reduced hydroxylase−regulatory protein complex of WT T4MO is depicted in the top panel. PyMOL was used to generate representations of the water network for mutant Q228A (bottom panel). The placement of these water molecules was selected to optimize the hydrogen-bonding distances between the water molecules and was supported by a previously reported X-ray crystallographic study.[37] In all representations, the hydroxylase is shown as a gray surface and the regulatory protein as a dark blue surface. The side chains of residues T201, N202, Q228X, and E231 are all drawn as sticks color coded according to atoms: carbon (teal), oxygen (red), nitrogen (blue), and iron (orange). Iron atoms and water molecules are shown as orange and red spheres, respectively.

form a model that would result in the observed kinetics. Loss of the carboxamide side chain in mutant Q228A may lead to the entry of water molecules into the pore. An unregulated flux of water molecules into the pore exposes the diiron center to more solvent, including H_3O^+, allowing for deactivation of oxygenated intermediates. In such a model, binding of ToMOD to mutant Q228A would not protect the diiron center from solvent access. This structural model would explain the sensitivity of mutant Q228A to protium−deuterium substitution, an increase in proton concentration, viscosity, and the diminish efficacy of ToMOD as a coupling protein. An alternative explanation for the observed kinetics is a change from classical PT in WT ToMOH to proton tunneling in

dx.doi.org/10.1021/bi500387y | *Biochemistry* 2014, 53, 3585−3592

mutant Q228A.[35,36] This possibility is highly disfavored owing to the relatively slow rate of turnover for steady-state reactivity.

For N202A, there is no significant KSIE or viscosity dependence during steady-state turnover, presumably because Q228 is sufficient to completely block the pore. Unfortunately, no direct evidence regarding proton transfer in WT ToMOH could be obtained through the studies presented here.

Residue Q228 Regulates Water Dissociation from the Diiron Active Site. Hydroxylation of substrates by BMMs involves the production of an alcohol or epoxide product and a water molecule. In addition, substrate binding[13] and a shifting glutamate residue[38] require expulsion of iron-bound water molecules from the active site by diffusion through the protein surface. Water flux through the interior of proteins typically proceeds through defined routes, frequently through hydrophilic channels.[39] The BMM pore is the only conserved, hydrophilic channel extending from the diiron center to the solvent-exposed surface.[12,14,16,38] Water egress cannot be directly monitored to determine whether the pore controls the flux, but indirect evidence is provided by the results of KSIE measurements.

Inverse solvent isotope effects in enzymology have been reported for cysteine protonation/deprotonation during catalysis[40,41] and water dissociation from metal ions.[42−44] Because there are no cysteine residues in proximity to the active site of ToMOH, the observed inverse isotope effects are assigned to release of water from the diiron active site during turnover. In particular, by protium−deuterium substitution, we observe inverse isotope effects for the KSIE(k_{cat}) of mutant Q228E and the KSIE(k_{cat}/K_m) of WT ToMOH and mutants N202A and Q228E.

For mononuclear cobalt,[44] iron,[45] and zinc,[46] the number of aqua or hydroxo ligands dissociating from a metal center can be calculated from the magnitude of the KSIE and fractionation factors (Φ, equilibrium distributions of the two isotopes). Fractionation factors for mononuclear centers have been previously reported. However, those factors for dimetallic centers are unreported to our knowledge. If each iron within the diiron active site is treated as a separate mononuclear center, surprising agreement is achieved between the experimental and predicted values (see the Supporting Information). From these data we conclude that water dissociation is rate-limiting for steady state turnover in mutant Q228E.

The KSIE(k_{cat}/K_m) values for mutants N202A and Q228E and for WT ToMOH are also less than 1, indicating that water dissociation from iron also contributes to rate constants comprising the KSIE(k_{cat}/K_m) values for these hydroxylase variants. For single-substrate enzymes, the k_{cat}/K_m incorporates rate constants for steps prior to the first irreversible one in the reaction pathway. In multisubstrate enzymes like ToMO, however, the order of substrate addition can change the composition of rate constants contributing to k_{cat}/K_m (Schemes S2 and S3 in the Supporting Information). Because of this complexity, changes in KSIE(k_{cat}/K_m) cannot be interpreted in terms of specific mechanistic changes or specific rate constants.

Binding of ToMOC to ToMOH Is Mediated by Pore Residues. We studied whether mutation of pore residues might effect a change in the reduction step of the catalytic cycle (Scheme 1). Mutants N202A and Q228E exhibited a decrease in rate constant for ET compared to WT ToMOH. The rate of interprotein electron transfer from $ToMOC_{red}$ to WT ToMOH is limited by the rate of protein association and cannot be saturated even at very high concentrations of ToMOH. Steady-state experiments demonstrate that the k_{cat} and k_{cat}/K_m values with respect to ToMOC are lower than those of WT ToMOH for all N202 and Q228 mutants. Taken together, these results show that N202 and Q228 are important for the function of ToMOC, most probably facilitating protein binding between the hydroxylase and the Rieske protein. If we consider dynamic interactions of the BMM hydroxylases, the regulatory proteins are known to bind over the pore in all X-ray crystallographically characterized BMM hydroxylase−regulatory protein complexes.[14−16] Thus, if ToMOC were also to bind at the pore, ToMOD and ToMOC must compete for an overlapping binding site on the surface of ToMOH.

Comparison of Putative Functions of the Pore in ToMOH and sMMOH. Mutation of Q228 to the analogous residue in sMMO, a glutamate, resulted in almost complete loss of steady-state activity and coupling efficiency. The most obvious conclusion is that the negative charge introduced significantly impacts the requisite conformational flexibility of this pore residue. However, the structurally analogous glutamate residue of sMMO, E240, undergoes a conformational rearrangement upon docking of the regulatory protein and hydroxylase despite its negative charge.[15] A comparison of crystal structures for ToMOH,[24] T4moH,[14] sMMOH,[47] and the hydroxylase−regulatory protein complexes for T4MO[14] and sMMO[15] revealed no amino acids surrounding the pore that would selectively stabilize a negatively charged versus a neutral species. The X-ray crystallographic study of mutant Q228E from T4MO offers a possible explanation.[37] In this investigation, the glutamine residue is able to stabilize HOH5, but mutation to glutamate results in loss of this water molecule.[37] If HOH5 and Q228 are involved in water release from the diiron active site, then mutant Q228E might exhibit low activity and coupling efficiency because its charge might retard the rate of water egress either by slowing the rate of conformational change or eliminating an essential hydrogen-bonding partner. The question of how sMMOH functions with a glutamate at this key position remains unanswered. Unlike in ToMOH and T4moH, sMMOH must release methanol during each catalytic cycle. It is possible that the pore of sMMOH is optimized for release of both water and methanol, whereas in other BMMs, the pore may be more specifically optimized for water release during catalytic turnover.

■ CONCLUSIONS

The role of a conserved pore near the diiron active site in BMMs, which opens and closes during catalysis,[14,15] has been a subject of much speculation, largely on the basis of static X-ray crystal structure information. Here, we unveil the role of pore residue Q228 through kinetic studies during catalysis. Through investigations of steady-state turnover, coupling efficiency, pH dependence, viscosity effect, and solvent kinetic isotope experiments, we determine that Q228 is critical for mediating water flux and attenuating PT, preventing adventitious attack on activated intermediates formed by the reaction of dioxygen with the reduced diiron(II) form of the hydroxylase. We postulate that it is the movement of this fluxional glutamine residue, opening and closing the pore, which conveys the observed functionality. Residue N202 of the pore is also critical for catalysis but is more important for protein−protein interaction, possibly stabilizing the conformations of Q228. Finally, we present evidence that the pore is near the binding interface of ToMOH:ToMOC, strongly supporting a com-

petitive binding model for the ToMOC and ToMOD components on the surface of ToMOH. The present work provides the first kinetic evidence regarding the function of a highly conserved pore in BMMs.

■ ASSOCIATED CONTENT

Supporting Information

Protein preparation details; proposed model for water dissociation from the diiron active site of Q228E; sequence alignment of alpha subunits of the hydroxylase proteins within BMMs; graphical descriptions of the NADH consumption, catechol formation, and quenched-activity assays; contributions to catalysis and the concentrations necessary to reach optimal catalytic activity of the component proteins used in the ToMO reactivity studies; reactions of each of the hydroxylase isoforms studied in H_2O and D_2O by the catechol formation assay; non-normalized data of the hydroxylase isoforms in varying concentrations of sucrose; reactions of each of the hydroxylase isoforms studied with varying concentration of ToMOC by the catechol formation assay; results from the quenched-activity and NADH assays; change in the extinction coefficient of ToMOC upon reduction with phosphate buffered dithionite; change of absorbance at 458 nm upon mixing $ToMOC_{red}$ with an oxidized hydroxylase isoform; size-exclusion chromatograms for binding between ToMOD-Fl and hydroxylase variants; hypothetical diagram depicting catalytic turnover of A of a bisubstrate reaction; and mathematical representation of the bisubstrate system. This material is available free of charge via the Internet at http://pubs.acs.org.

■ AUTHOR INFORMATION

Corresponding Author

*E-mail: lippard@mit.edu. Telephone: (617) 253-1892. Fax: (617) 258-8150.

Funding

This work was funded by the National Institute of General Medical Sciences under grant 2R01-GM032113. A.D.L. thanks the National Institutes of Health for partial support under Interdepartmental Biotechnology Training Grant T32 GM008334.

Notes

The authors declare no competing financial interest.

■ ACKNOWLEDGMENTS

We thank Dr. Woon Ju Song, Kanchana Ravichandran, and Weixue Wang for helpful discussions.

■ ABBREVIATIONS USED

BMM, bacterial multicomponent monooxygenase; NAD(P)H, reduced nicotinamide adenine dinucleotide (also NADH) or reduced nicotinamide adenine dinucleotide phosphate; PT, proton transfer; ET, electron transfer; ToMO, toluene/*o*-xylene monooxygenase; ToMOH, hydroxylase component of ToMO; ToMOD, cofactorless regulatory component of ToMO; ToMOD-Fl, fluorescein-labeled ToMOD; ToMOC, Rieske-type ferredoxin of ToMO; ToMOF, NADH-oxidoreductase of ToMO; sMMO, soluble methane monooxygenase; sMMOH, hydroxylase component of sMMO; WT, wild type; C23O, catechol-2,3-dioxygenase; T4MO, toluene-4-monooxygenase; T4moH, hydroxylase component of T4MO; T4moD, cofactorless regulatory component of T4MO; ToMOD-Fl, fluorescein-labeled ToMOD; Tris, tris(hydroxymethyl)-aminomethane; Bis-Tris propane, bis(tris(hydroxymethyl)methylamino)-propane; $ToMOC_{red}$, reduced ToMOC; $ToMOC_{ox}$, oxidized ToMOC; KSIE, kinetic solvent isotope effect

■ REFERENCES

(1) Nazaries, L., Murrell, J. C., Millard, P., Baggs, L., and Singh, B. K. (2013) Methane, Microbes and Models: Fundamental Understanding of the Soil Methane Cycle for Future Predictions. *Environ. Microbiol. 15*, 2395−2417.

(2) Holmes, A. J. (2009) Advances in Applied Bioremediation, in *Advances in Applied Bioremediation* (Singh, A., Kuhad, R. C., and Ward, O. P., Eds.) pp 91−101.

(3) Papa, R., Parrilli, E., and Sannia, G. (2009) Engineered Marine Antarctic Bacterium *Pseudoalteromonas haloplanktis* TAC125: A Promising Micro-organism for the Bioremediation of Aromatic Compounds. *J. Appl. Microbiol. 106*, 49−56.

(4) Notomista, E., Lahm, A., Di Donato, A., and Tramontano, A. (2003) Evolution of Bacterial and Archaeal Multicomponent Monooxygenases. *J. Mol. Evol. 56*, 435−445.

(5) Gassner, G. T., and Lippard, S. J. (1999) Component Interactions in the Soluble Methane Monooxygenase System from *Methylococcus capsulatus* (Bath). *Biochemistry 38*, 12768−12785.

(6) Moe, L. A., McMartin, L. A., and Fox, B. G. (2006) Component Interactions and Implications for Complex Formation in the Multicomponent Toluene 4-Monooxygenase. *Biochemistry 45*, 5478−5485.

(7) Tinberg, C. E., Song, W. J., Izzo, V., and Lippard, S. J. (2011) Multiple Roles of Component Proteins in Bacterial Multicomponent Monooxygenases: Phenol Hydroxylase and Toluene/*o*-Xylene Monooxygenase from *Pseudomonas* sp. OX1. *Biochemistry 50*, 1788−1798.

(8) Leahy, J. G., Batchelor, P. J., and Morcomb, S. M. (2003) Evolution of the Soluble Diiron Monooxygenases. *FEMS Microbiol. Rev. 27*, 449−479.

(9) Murray, L. J., and Lippard, S. J. (2007) Substrate Trafficking and Dioxygen Activation in Bacterial Multicomponent Monooxygenases. *Acc. Chem. Res. 40*, 466−474.

(10) Song, W. J., Gucinski, G., Sazinsky, M. H., and Lippard, S. J. (2011) Tracking a Defined Route for O_2 Migration in a Dioxygen-Activating Diiron Enzyme. *Proc. Natl. Acad. Sci. U.S.A. 108*, 14795−14800.

(11) McCormick, M. S., and Lippard, S. J. (2011) Analysis of Substrate Access to Active Sites in Bacterial Multicomponent Monooxygenase Hydroxylases: X-ray Crystal Structure of Xenon-Pressurized Phenol Hydroxylase from *Pseudomonas* sp. OX1. *Biochemistry 50*, 11058−11069.

(12) Whittington, D. A., Rosenzweig, A. C., Frederick, C. A., and Lippard, S. J. (2001) Xenon and Halogenated Alkanes Track Putative Substrate Binding Cavities in the Soluble Methane Monooxygenase Hydroxylase. *Biochemistry 40*, 3476−3482.

(13) Bailey, L. J., Acheson, J. F., McCoy, J. G., Elsen, N. L., Phillips, G. N., and Fox, B. G. (2012) Crystallographic Analysis of Active Site Contributions to Regiospecificity in the Diiron Enzyme Toluene 4-Monooxygenase. *Biochemistry 51*, 1101−1113.

(14) Bailey, L. J., McCoy, J. G., Phillips, G. N., and Fox, B. G. (2008) Structural Consequences of Effector Protein Complex Formation in a Diiron Hydroxylase. *Proc. Natl. Acad. Sci. U.S.A. 105*, 19194−19198.

(15) Lee, S. J., McCormick, M. S., Lippard, S. J., and Cho, U.-S. (2013) Control of Substrate Access to the Active Site in Methane Monooxygenase. *Nature 494*, 380−384.

(16) Sazinsky, M. H., Dunten, P. W., McCormick, M. S., DiDonato, A., and Lippard, S. J. (2006) X-ray Structure of a Hydroxylase-Regulatory Protein Complex from a Hydrocarbon-Oxidizing Multicomponent Monooxygenase *Pseudomonas* sp. OX1 Phenol Hydroxylase. *Biochemistry 45*, 15392−15404.

(17) Cafaro, V., Notomista, E., Capasso, P., and Di Donato, A. (2005) Regiospecificity of Two Multicomponent Monooxygenases from *Pseudomonas stutzeri* OX1: Molecular Basis for Catabolic

Adaptation of this Microorganism to Methylated Aromatic Compounds. *Appl. Environ. Microbiol. 71*, 4736−4743.
(18) Cafaro, V., Scognamiglio, R., Viggiani, A., Izzo, V., Passaro, I., Notomista, E., Dal Piaz, F., Amoresano, A., Casbarra, A., Pucci, P., and Di Donato, A. (2002) Expression and Purification of the Recombinant Subunits of Toluene/*o*-Xylene Monooxygenase and Reconstitution of the Active Complex. *Eur. J. Biochem. 269*, 5689−5699.
(19) *The PyMOL Molecular Graphics System*, version 1.3, Schrödinger, LLC.
(20) Song, W. J., Behan, R. K., Naik, S. G., Huynh, B. H., and Lippard, S. J. (2009) Characterization of a Peroxodiiron(III) Intermediate in the T201S Variant of Toluene/*o*-Xylene Monooxygenase Hydroxylase from *Pseudomonas sp.* OX1. *J. Am. Chem. Soc. 131*, 6074−6075.
(21) Cook, P. F., and Cleland, W. W. (2007) *Enzyme Kinetics and Mechanism*, Garland Science, London.
(22) Schmidt, D. E., and Westheimer, F. H. (1971) p*K* of the Lysine Amino Group at the Active Site of Acetoacetate Decarboxylase. *Biochemistry 10*, 1249−1253.
(23) Harris, K. R., and Woolf, L. A. (2004) Temperature and Volume Dependence of the Viscosity of Water and Heavy Water at Low Temperatures. *J. Chem. Eng. Data 49*, 1064−1069.
(24) Sazinsky, M. H., Bard, J., Di Donato, A., and Lippard, S. J. (2004) Crystal Structure of the Toluene/*o*-Xylene Monooxygenase Hydroxylase from *Pseudomonas stutzeri* OX1 − Insight into the Substrate Specificity, Substrate Channeling, and Active Site Tuning of Multicomponent Monooxygenases. *J. Biol. Chem. 279*, 30600−30610.
(25) Elsen, N. L., Bailey, L. J., Hauser, A. D., and Fox, B. G. (2009) Role for Threonine 201 in the Catalytic Cycle of the Soluble Diiron Hydroxylase Toluene 4-Monooxygenase. *Biochemistry 48*, 3838−3846.
(26) Pikus, J. D., Mitchell, K. H., Studts, J. M., McClay, K., Steffan, R. J., and Fox, B. G. (2000) Threonine 201 in the Diiron Enzyme Toluene 4-Monooxygenase Is Not Required for Catalysis. *Biochemistry 39*, 791−799.
(27) Song, W. J., and Lippard, S. J. (2011) Mechanistic Studies of Reactions of Peroxodiiron(III) Intermediates in T201 Variants of Toluene/*o*-Xylene Monooxygenase Hydroxylase. *Biochemistry 50*, 5391−5399.
(28) Song, W. J., McCormick, M. S., Behan, R. K., Sazinsky, M. H., Jiang, W., Lin, J., Krebs, C., and Lippard, S. J. (2010) Active Site Threonine Facilitates Proton Transfer during Dioxygen Activation at the Diiron Center of Toluene/*o*-Xylene Monooxygenase Hydroxylase. *J. Am. Chem. Soc. 132*, 13582−13585.
(29) Murray, L. J., Naik, S. G., Ortillo, D. O., Garcia-Serres, R., Lee, J. K., Huynh, B. H., and Lippard, S. J. (2007) Characterization of the Arene-Oxidizing Intermediate in ToMOH as a Diiron(III) Species. *J. Am. Chem. Soc. 129*, 14500−14510.
(30) Fox, B. G., Froland, W. A., Dege, J. E., and Lipscomb, J. D. (1989) Methane monooxygenase from *Methylosinus trichosporium* OB3b. Purification and Properties of a Three-Component System with High Specific Activity from a Type II Methanotroph. *J. Biol. Chem. 264*, 10023−10033.
(31) Fox, B. G., Liu, Y., Dege, J. E., and Lipscomb, J. D. (1991) Complex Formation between the Protein Components of Methane Monooxygenase from *Methylosinus trichosporium* Ob3b − Identification of Sites of Component Interaction. *J. Biol. Chem. 266*, 540−550.
(32) Pocker, Y., and Janjić, N. (1987) Enzyme Kinetics in Solvents of Increased Viscosity. Dynamic Aspects of Carbonic Anhydrase Catalysis. *Biochemistry 26*, 2597−2606.
(33) Holm, R. H., Kennepohl, P., and Solomon, E. I. (1996) Structural and Functional Aspects of Metal Sites in Biology. *Chem. Rev. 96*, 2239−2314.
(34) Tinberg, C. E., and Lippard, S. J. (2009) Revisiting the Mechanism of Dioxygen Activation in Soluble Methane Monooxygenase from *M. capsulatus* (Bath): Evidence for a Multi-Step, Proton-Dependent Reaction Pathway. *Biochemistry 48*, 12145−12158.
(35) Kohen, A., and Klinman, J. P. (1999) Hydrogen Tunneling in Biology. *Chem. Biol. 6*, R191−R198.
(36) Sharma, S. C., and Klinman, J. P. (2008) Experimental Evidence for Hydrogen Tunneling when the Isotopic Arrhenius Prefactor (A_H/A_D) is Unity. *J. Am. Chem. Soc. 130*, 17632−17633.
(37) Bailey, L. J. (2009) Ph.D. Dissertation, Structural Insight into Protein Complex Formation and Reaction Mechanism of Toluene 4-Monooxygenase, University of Wisconsin−Madison, Madison, WI.
(38) McCormick, M. S., Sazinsky, M. H., Condon, K. L., and Lippard, S. J. (2006) X-ray Crystal Structures of Manganese(II)-Reconstituted and Native Toluene/*o*-Xylene Monooxygenase Hydroxylase Reveal Rotamer Shifts in Conserved Residues and an Enhanced View of the Protein Interior. *J. Am. Chem. Soc. 128*, 15108−15110.
(39) Miao, Y., and Baudry, J. (2011) Active-Site Hydration and Water Diffusion in Cytochrome P450cam: A Highly Dynamic Process. *Biophys. J. 101*, 1493−1503.
(40) Belasco, J. G., Bruice, T. W., Albery, W. J., and Knowles, J. R. (1986) Energetics of Proline Racemase: Fractionation Factors for the Essential Catalytic Groups in the Enzyme−Substrate Complexes. *Biochemistry 25*, 2558−2564.
(41) Weiss, P. M., Cook, P. F., Hermes, J. D., and Cleland, W. W. (1987) Evidence from Nitrogen-15 and Solvent Deuterium Isotope Effects on the Chemical Mechanism of Adenosine Deaminase. *Biochemistry 26*, 7378−7384.
(42) Flagg, S. C., Giri, N., Pektas, S., Maroney, M. J., and Knapp, M. J. (2012) Inverse Solvent Isotope Effects Demonstrate Slow Aquo Release from Hypoxia Inducible Factor-Prolyl Hydroxylase (PHD2). *Biochemistry 51*, 6654−6666.
(43) Harrison, R. K., Chang, B., Niedzwiecki, L., and Stein, R. L. (1992) Mechanistic Studies on the Human Matrix Metalloproteinase Stromelysin. *Biochemistry 31*, 10757−10762.
(44) Kassebaum, J. W., and Silverman, D. N. (1989) Hydrogen/Deuterium Fractionation Factors of the Aqueous Ligand of Cobalt in $Co(H_2O)_6^{2+}$ and Co(II)-Substituted Carbonic Anhydrase. *J. Am. Chem. Soc. 111*, 2691−2696.
(45) Hangasky, J. A., Saban, E., and Knapp, M. J. (2013) Inverse Solvent Isotope Effects Arising from Substrate Triggering in the Factor Inhibiting Hypoxia Inducible Factor. *Biochemistry 52*, 1594−1602.
(46) Cook, P. F. (1991) *Enzyme Mechanism from Isotope Effects*, pp 40−42, 83−116, and 160, CRC Press, Boca Raton, FL.
(47) Rosenzweig, A. C., Frederick, C. A., Lippard, S. J., and Nordlund, P. (1993) Crystal Structure of a Bacterial Non-Haem Iron Hydroxylase that Catalyzes the Biological Oxidation of Methane. *Nature 366*, 537−543.